COMPUTATIONAL MODELING OF CRACK PROPAGATION IN FRACTURED ROCKS USING FINITE ELEMENTS WITH HIGH ASPECT RATIO

Heber A. A. Fabbri

Pedro R. Cleto

Eduardo A. Rodrigues

José H. K. Ambiel

Osvaldo L. Manzoli

heber.fabbri@feb.unesp.br

pedro.cleto@feb.unesp.br

eduardoalex@feb.unesp.br

zeambiel@hotmail.com

omanzoli@feb.unesp.br

Mechanical Engineering Department - São Paulo State University - UNESP

Avenida Engenheiro Luiz Edmundo Coube 14-01, 17033-360, Bauru, São Paulo, Brasil

Abstract. *This work presents a numerical method to modeling rocks containing pre-existing fracture networks. In this approach, the nonlinear behavior of the material is modeled in the context of the Finite Element Method (FEM), using the called Mesh Fragmentation Technique (MFT), which is based on the use of solid interface finite elements with high aspect ratio. These interface elements present the same kinematics as the continuous strong discontinuity approach (CSDA), being suitable to represent the formation of discontinuities associated with cracks. The pre-existing fractures are explicitly represented in the continuous material by employing these interface elements, which are strategically positioned according to the geometry of the fracture network in the FE mesh. Thus, appropriate constitutive models are adopted to describe the complex failure behavior of material due to the influence of pre-existing fractures. Aiming to better understand the influence of the natural fractures on the failure process, the proposed model is applied to study the effect of individual and random multiple pre-existing fractures on the mechanical behavior of blocks under uniaxial tensile and compression load.*

Keywords: *Interface finite element, Constitutive contact model, Natural fractures, Rocks*

1 INTRODUCTION

A good understanding on the influence of natural fractures on the behavior of rock masses is fundamental to describe the performance of a discontinuous rock mass under changing stress conditions. According to Bandis et al. (1983), at the relatively low stress levels encountered in near-surface excavations, the deformation of joints dominates the elastic deflection of the intact rock. Even under the higher levels of stress associated with heavy structures, the slippage and closure of joints constitute the major part of settlement on rock.

In the context of Finite Element analysis, the formation and propagation of discontinuities associated with cracks in the interior of the finite elements (in an originally continuum solid) can be described via Embedded Crack Elements (E-FEM) or Extended Finite Elements (X-FEM). In both methods, techniques to track the crack path during the analysis are required, in order to provide information about the position of the crack surfaces for the corresponding discontinuous kinematic enrichment. Although these techniques are relatively simple to represent a few cracks in 2D analyses, they become very complex and even unsuitable for problems involving multiple crack surfaces in 3D analysis (Jager et al., 2008; Manzoli et al., 2013; Oliver et al., 2004).

Therefore, in order to avoid the necessity of crack tracking schemes, a technique based on the insertion of special interface elements in between regular elements of the mesh is adopted. These interface elements must be able to describe the kinematics associated to discontinuities, so that the crack formation can develop along the boundaries of the regular elements.

Instead of using zero-thickness interface elements with discrete (cohesive) constitutive models, relating relative displacement with interface stresses (Pandolfi and Ortiz, 2002; Camacho and Ortiz, 1996; Caballero et al., 2006), this work employs the tecnique proposed by Manzoli et al. (2012) and Manzoli et al. (2014), which models these interfaces by means of degenerated solid finite elements, i.e., elements with a very high aspect ratio (ratio of the largest to the smallest dimension), with the smallest dimension corresponding to the thickness of the interface region. As the aspect ratio of the element increases, the element strains also increase, approaching the kinematics of the strong discontinuity, as is the case of the Continuous Strong Discontinuity Approach (CSDA).

A tensile damage constitutive relation between strains and stresses, compatible with the CSDA, is employed to describe the nonlinear behavior of the interfaces. With this model the interface elements can transfer normal (compressive) stresses without overlapping. Also, this work proposes the use of interface elements to describe the behavior of natural fractures present on rock masses. A suitable constitutive model, based on the joint model proposed by Bandis et al. (1983), is proposed to describe the behavior of natural fractures under compressive load.

With this technique the analyses are performed integrally in the context of the continuum mechanics and complex crack patterns involving multiple cracks can be simulated without the need of tracking algorithms. This work also proposes the use of the interface elements to describe the natural fractures present in rocks.

2 SOLID INTERFACE FINITE ELEMENT

Consider the three-node solid finite element with base b given by the line segment between nodes 2 and 3, and height h, given by the distance between the node 1 and its projection on the base $1'$, as illustrated in Fig. 1. According to the local Cartesian coodinate system (n, s), with the s-axis parallel to the element base and the n-axis ortogonal to the element base, the coordinates of the element nodes 1, 2 and 3 are given by:

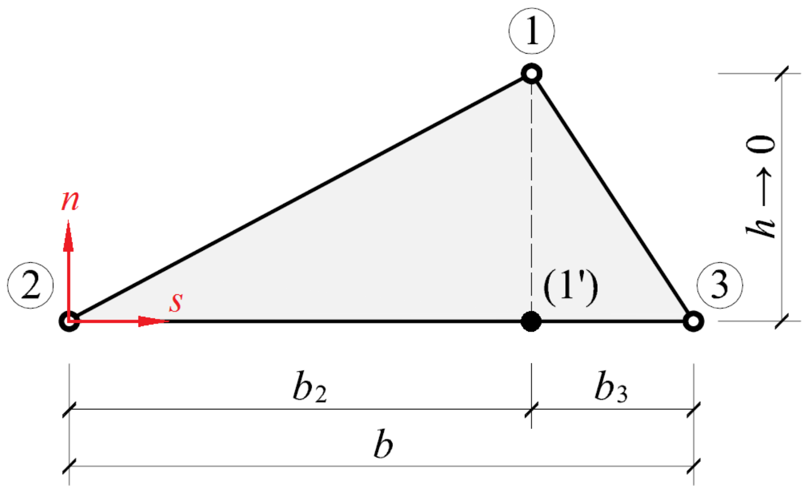

Figure 1: Three nodes solid finite element with high aspect ratio (adapted from Manzoli et al. (2012)).

$$\begin{cases} \mathbf{x}^{(1)} = (\alpha b, h) \\ \mathbf{x}^{(2)} = (0, 0) \\ \mathbf{x}^{(3)} = (b, 0) \end{cases} \tag{1}$$

where $\alpha = b_2/b$. The strain tensor for any point of the element can be approximated, in plane strain problems, by:

$$\boldsymbol{\epsilon} = \hat{\boldsymbol{\epsilon}} + \tilde{\boldsymbol{\epsilon}}, \tag{2}$$

with

$$\tilde{\boldsymbol{\epsilon}} = \frac{1}{b} \begin{bmatrix} 0 & \frac{1}{2}\left(u_n^{(3)} - u_n^{(2)}\right) & 0 \\ \frac{1}{2}\left(u_n^{(3)} - u_n^{(2)}\right) & 0 & 0 \\ 0 & 0 & 0 \end{bmatrix} \tag{3}$$

and

$$\hat{\boldsymbol{\epsilon}} = \frac{1}{h} \begin{bmatrix} [\![u]\!]_n & \frac{1}{2}[\![u]\!]_s & 0 \\ \frac{1}{2}[\![u]\!]_s & 0 & 0 \\ 0 & 0 & 0 \end{bmatrix}, \tag{4}$$

where $u_n^{(i)}$ and $u_s^{(i)}$ are the displacement components of the node i according to the (n, s) coordinade local system, $[\![u]\!]_n = u_n^{(1)} - u_n^{(1')}$ and $[\![u]\!]_s = u_s^{(1)} - u_s^{(1')}$ are the components of the relative displacement, $[\![\mathbf{u}]\!]$, between node 1 and its corresponding projection on the base $(1')$:

$$[\![u]\!]_n = u_n^{(1)} - u_n^{(1')} = u_n^{(1)} - \left[\alpha u_n^{(3)} + (1-\alpha) u_n^{(2)}\right], \tag{5}$$

$$[\![u]\!]_s = u_s^{(1)} - u_s^{(1')} = u_s^{(1)} - \left[\alpha u_s^{(3)} + (1-\alpha) u_s^{(2)}\right]. \tag{6}$$

The displacement of the projection point $(1')$ in Eq. (5) and (6) was obtained by interpolating the displacements of nodes 2 and 3. Also, the strain part given by Eq. (4) can be rewritten, for any coordinate system, as:

$$\hat{\boldsymbol{\epsilon}} = \frac{1}{h} \left(\mathbf{n} \otimes [\![\mathbf{u}]\!]\right)^s, \tag{7}$$

where $(\bullet)^s$ refers to the symmetric part of $(\bullet)$, $\mathbf{n}$ is the unit vector ortogonal to the element base and $\otimes$ denotes the diatic product. Hence, the total strain tensor in Eq. (2) becomes:

$$\boldsymbol{\epsilon} = \tilde{\boldsymbol{\epsilon}} + \underbrace{\frac{1}{h} \left(\mathbf{n} \otimes [\![\mathbf{u}]\!]\right)^s}_{\hat{\boldsymbol{\epsilon}}}. \tag{8}$$

When the height h tends to zero, the strain component $\tilde{\boldsymbol{\epsilon}}$ remains bounded while the component $\hat{\boldsymbol{\epsilon}}$ is no longer bounded. Therefore, in the limit situation of h tending to zero, the element strains are related almost exclusively to the relative displacement between node 1 and its projection on the element base,$[\![\mathbf{u}]\!]$. Also, is importante to note that in the limit situation, node 1 tend to the same material point of its projection. As a consequence, the relative displacement $[\![\mathbf{u}]\!]$ becomes the measure of a displacement discontinuity (strong discontinuity).

The structure of the strain field in Eq. (8) corresponds to the typical kinematics of the continuous strong discontinuity approach (CSDA). Therefore, the same applications of the CSDA can be treated with triangular finite elements with high aspect ratio (ratio of the largest to the smallest dimension, given by b/h) (Manzoli et al., 2012, 2014).

3 CONTINUUM CONSTITUTIVE MODEL

It is well know that constitutive models based on the Continuum Damage Mechanics Theory (CDMT) are appropriate to describe the material degradation process due to crack propagation in brittle materials, like rocks and concrete. For this class of models, the mechanical behavior of a damaged material is usually described in the field of the effective stress, together with the hypothesis of mechanical equivalence between the damage and the undamaged material.

In this work, a suitable tension damage model proposed by Manzoli et al. (2012) is adopted to describe the phenomenon of crack initiation and propagation through the interface solid finite elements, using the component of the stress normal to the element base as a damage criterion. To describe the deformation of natural fractures under compressive stresses a new model is proposed, based on the tension damage model and on the Barton-Bandis joint model (Bandis et al., 1983).

3.1 Tension damage model

The tension damage model, proposed by Manzoli et al. (2012), is defined by the following constitutive relation:

$$\boldsymbol{\sigma} = (1-d)\underbrace{\mathbb{C} : \boldsymbol{\epsilon}}_{\bar{\boldsymbol{\sigma}}}, \tag{9}$$

where $\boldsymbol{\sigma}$ is the nominal stress, $0 \leq d \leq 1$ is the scalar damage variable, $\mathbb{C}$ is the fourth order elastic tensor and the product $\mathbb{C} : \boldsymbol{\epsilon}$ defines the effective stress tensor $\bar{\boldsymbol{\sigma}}$.

The damage criterion that defines the elastic domain is given by:

$$\phi^d = \sigma_{nn} - q^d(r^d) \leq 0, \tag{10}$$

where σ_{nn} is the component of the stress normal to the base of the element ($\sigma_{nn} = \mathbf{n} \cdot \boldsymbol{\sigma} \cdot \mathbf{n}$), q^d and r^d are the stress and strain-like internal variables, respectively.

The damage criterion can be expressed in terms of the effective stress dividing Eq. (10) by $(1-d)$:

$$\bar{\phi}^d = \bar{\sigma}_{nn} - r^d \leq 0, \tag{11}$$

where $r^d = q^d/(1-d)$ controls the size of the elastic domain in the space of the effective stress. Thus, a damage evolution rule can be defined in terms of the internal variable r^d:

$$d(r^d) = 1 - \frac{q^d(r^d)}{r^d}. \tag{12}$$

The constitutive model is completed by the loading-unloading conditions, given by the Kuhn-Tucker relations:

$$\bar{\phi}^d \leq 0, \dot{r}^d \geq 0, \dot{r}^d\bar{\phi}^d = 0, \tag{13}$$

and the consistency condition

$$\dot{r}^d\dot{\bar{\phi}}^d = 0 \quad \text{if} \quad \bar{\phi}^d = 0. \tag{14}$$

Eqs. (14) and (11) lead to a explicit evolution law for the strain-like internal variable along the pseudo-time t associated with the loading process, given by:

$$r^d_t = \max_{s\in[0,t]}[\bar{\sigma}_{nn}, r^d_0]. \tag{15}$$

According to Eq. (15), r^d takes the maximum value that the effective tensile stress $\bar{\sigma}_{nn}$ reaches during the loading process, starting from the initial value, r^d_0, equal to the material tensile strength f_t. The following exponencial softening law was adopted here:

$$q^d(r^d) = q^d_0 e^{Ah(1-\frac{r^d}{q^d_0})}, \qquad \text{with} \quad q^d_0 = f_t, \tag{16}$$

where A is the softening parameter. When h tends to zero, the mode I fracture energy G_f, i.e., the energy dissipated in a complete degradation of the interface element in mode I, relates to the softening parameter by:

$$G_f = \frac{f_t^2}{AE} \tag{17}$$

where E is the material Young's modulus.

3.2 Contact model

The behavior of the pre-existing natural fractures on rocks under changing compressive stresses is discribed in terms of the Barton-Bandis joint (Bandis et al., 1983), which suggest a non-linear relation between the normal compressive stress σ_{nn} acting on the fracture and the normal relative displacement $[\![u]\!]_n$. The proposed relation between σ_{nn} and $[\![u]\!]_n$ resembles a hiperbola, and is given by the equation:

$$\sigma_{nn} = \frac{k_{ni} V_m [\![u]\!]_n}{V_m - [\![u]\!]_n}, \tag{18}$$

where k_{ni} is the initial normal stiffness, and V_m is the maximum closure of the fractures walls, or the maximum value of $[\![u]\!]_n$. Based on the tensile damage model proposed by Manzoli et al. (2012) and on the Barton-Bandis joint model, a "contact" model is proposed to describe the fractures closure.

Consider the continuum model given by the constitutive relation:

$$\boldsymbol{\sigma} = \xi \mathbb{C} : \boldsymbol{\epsilon}, \tag{19}$$

where $0 \leq \xi \leq 1$ is a contact internal variable which increases according to fracture closure. The contact criterion the defines the elastic domain is given by:

$$\phi^c = -\sigma_{nn} + q^c(r^c) \leq 0, \tag{20}$$

where q^c and r^c are the stress and strain-like internal variables, respectively. The contact criterion can be expressed in terms of effective stresses dividing the Eq. (20) by ξ:

$$\bar{\phi}^c = -\bar{\sigma}_{nn} + r^c \leq 0, \tag{21}$$

with

$$r^c = \frac{q^c(r^c)}{\xi}. \tag{22}$$

The evolution law for the strain-like internal variable along the pseudo-time t associated with the loading process is given by:

$$r^c_t = \max_{s \in [0,t]} [-\bar{\sigma}_{nn}, 0]. \tag{23}$$

During the loading process, the value of the contact internal variable r^c starts with 0 and assumes the maximum compression stress value reached by the elastic stress tensor component σ_{nn}. Finally, based on Eq. (18), the evolution of the q^c variable is given by:

$$q^c(r^c) = \frac{k_{ni} V_m}{\left(\dfrac{V_m E}{h} - r^c \right)} r^c, \tag{24}$$

where E is the Young's modulus of the rock.

4 NUMERICAL RESULTS

The proposed examples aim to demonstrate the ability of the adopted technique to describe both the closure process on compressed natural fractures and the crack propagation of fractures under tensile stress. All the exemples consist on uniaxial load. The rock material properties for the examples are given in Table 1 and the fractures properties in Table 2. The finite elements representing rocks on the meshes of the examples are colored in light brown, the interface elements representing the natural fractures are colored grey and the ones representing the cracks are colored black.

Table 1: Rock properties

Propertie	Nomenclature	Value
Young's modulus (GPa)	E	21.0
Poisson's ratio (-)	ν	0.0
Tensile strength (MPa)	f_t	3.0
Fracture energy (N/m)	G_f	100.0

Table 2: Natural fractures properties

Propertie	Nomenclature	Value
Young's modulus (GPa)	E	2.1
Poisson's ratio (-)	ν	0.0
Tensile strength (MPa)	f_t	0.001
Fracture energy (N/m)	G_f	100.0
Initial stiffness (MPa/mm)	k_{ni}	100.0
Maximum closure (mm)	V_m	0.1

4.1 Interface element

This example aims to demonstrate the tensile damage model. Consider a 10×20 cm block, as shown in the Fig. 2(a), with Young's modulus $E = 2.1$GPa, Poisson's ratio $\nu = 0$, tensile strength $f_t = 3$MPa and fracture energy $G_f = 50$N/m. The mesh used in the simulation (Fig. 2(b)) contain a pair of interface elements placed in the middle part of the block. Tensile and compressive uniaxial loads were applied to the block by imposing positive and negative vertical displacements $\bar{u}_n$ as shown on Fig. 2(a). Figure 2(c) shows the evolution of the normal stress σ_{nn} with respect to the imposed displacement. As the tensile load is applied on the block, the material presents linear relation between stress and relative displacement with $[\![u]\!]_n$ tending to zero, until the tensile stress reaches the material tensile strenght, when the material starts to degrade and presents non-linear behavior. Once the positive relative displacement is removed, the stress returns linearly to the origin, in agreement with the damage theory. As this model only consider damage caused by tensile stress (see the damage criterion, Eq. (10)), when a compressive load is applied the stress varies linearly with the relative displacement, with the same behavior as the non danified material. This occurs because this model only describes material damage under tensile stress.

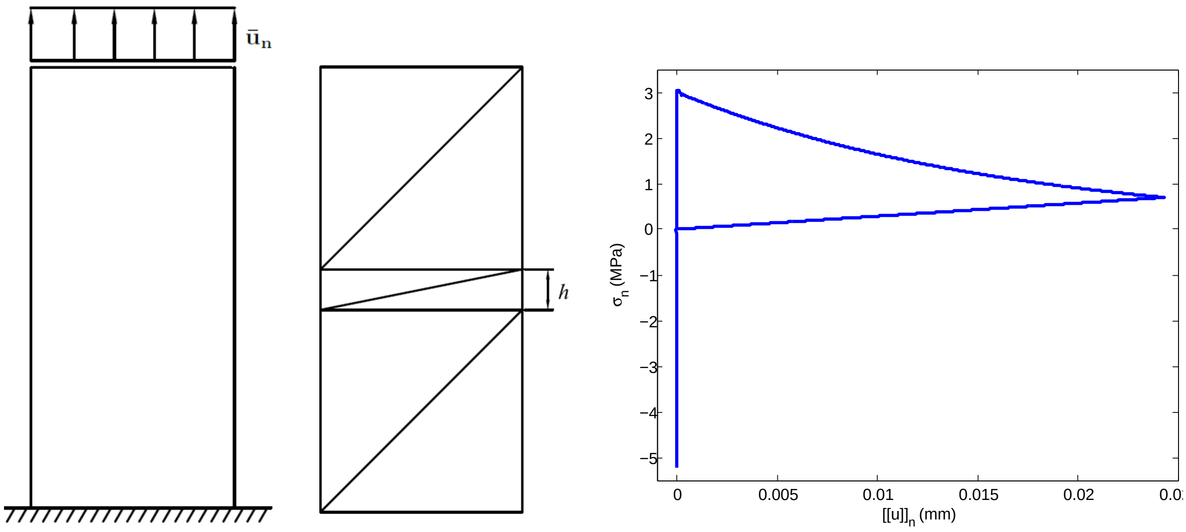

(a) (b) (c)

Figure 2: 10×20 cm size block under uniaxial load. a)Boundary conditions. b) Mesh. c) Normal stress vs normal relative displacement

4.2 Rock block containing a single fracture under tensile loading

Consider a rock block of 100×100 m containing one natural fracture, as shown on Fig. 3. A tensile uniaxial load was applied by imposing vertical displacement on the upper face of the block. To show that the proposed technique is able to represent the behavior of natural fractures under tensile stresses, first consider the rock with elastic behavior. As shown on Fig. 3(c), the fracture can freely open. Figure 4 shows the same test, but using the proposed model to allow crack propagation on the rock. As it can be seen, crack propagates from the fracture tips and as a consequence a fracture growth is observed, which demonstrate that the employed technique is able to describe deformation and growth under tensile loading.

4.3 Rock block containing a single fracture under compressive loading

The same rock block from the example 4.2 was submited to a compressive load. The deformation of the natural fracture is given by the Eq. (18). As the fracture walls become closer to each other, the contact area between the asperities of the walls increases, causing a increase on the compressive stiffnes of the fracture, which justify the hiperbolic relationship between the normal component of stress and the normal relative displacement. The proposed contact model is able to represent this behavior, as shown on Fig. 5(b), where a comparison between the theoretical curve given by Eq. (18) and the numerical curve obtained with the proposed contact model. The results show a good agreement with the theoretical curve.

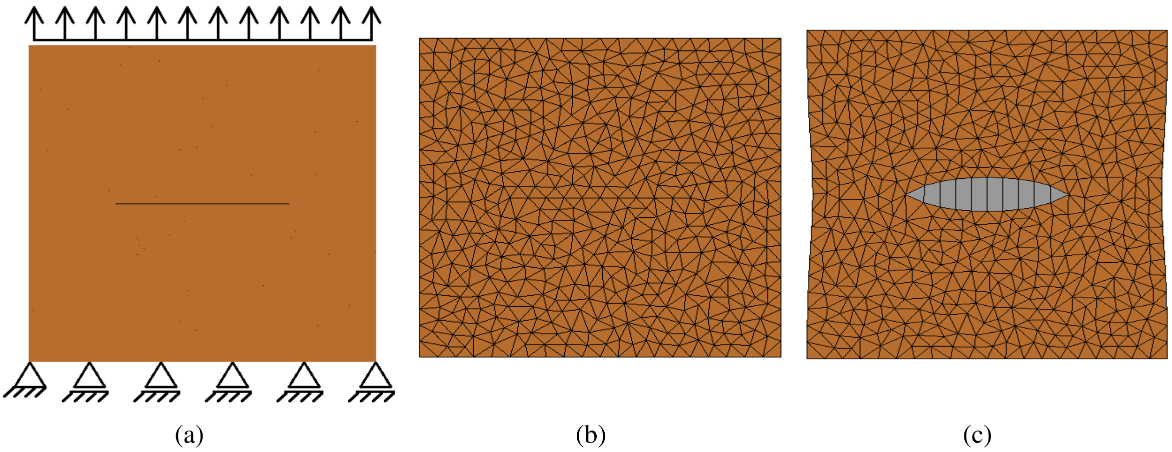

Figure 3: Rock block containing a single fracture under tensile loading. (a) Boundary conditions. (b) Finite elements mesh. (c) Response with elastic behavior

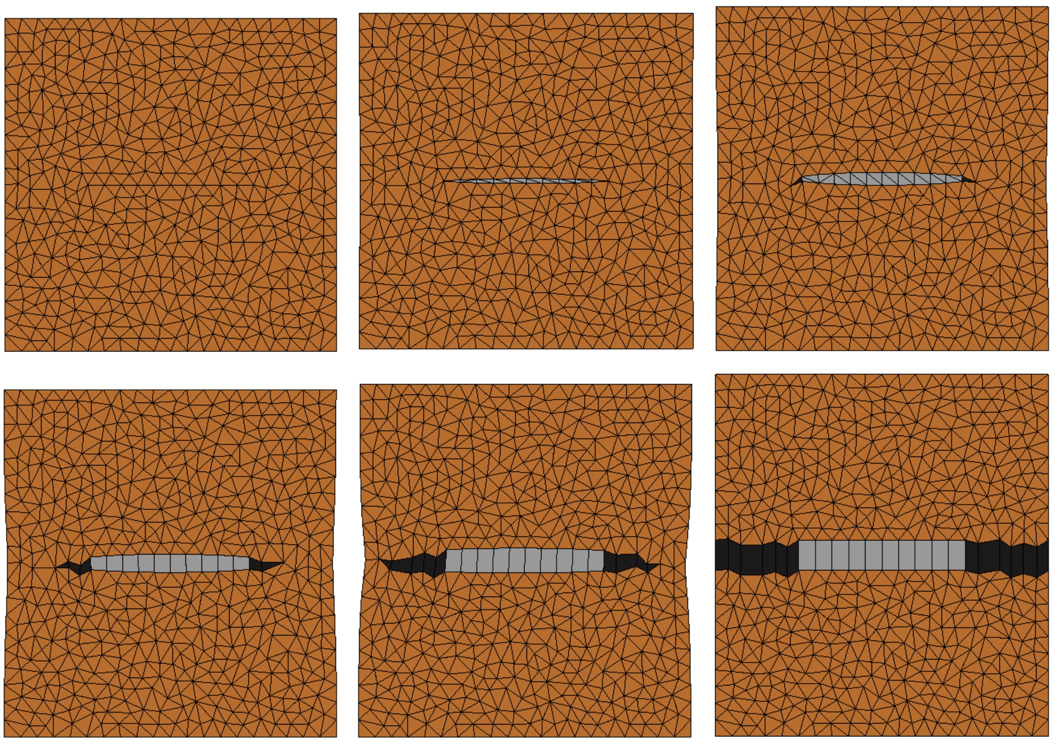

Figure 4: Single fractured rock with the proposed model under tensile loading

4.4 Rock block containing multiples fractures

A rock block of 100×100 m with multiples natural fractures was submited to a tensile axial loading, as shown on Fig. 6(a). All the fractures are represented by solid interface elements with the properties of Table 2. The tensile uniaxial loading was applied by imposing vertical displacement on the upper face of the block.

Figure 6 shows that the proposed model is able to simulate the propagation of the natural fractures. The cracks propagation enables that some fractures connect to others, creating a net of connected fractures.

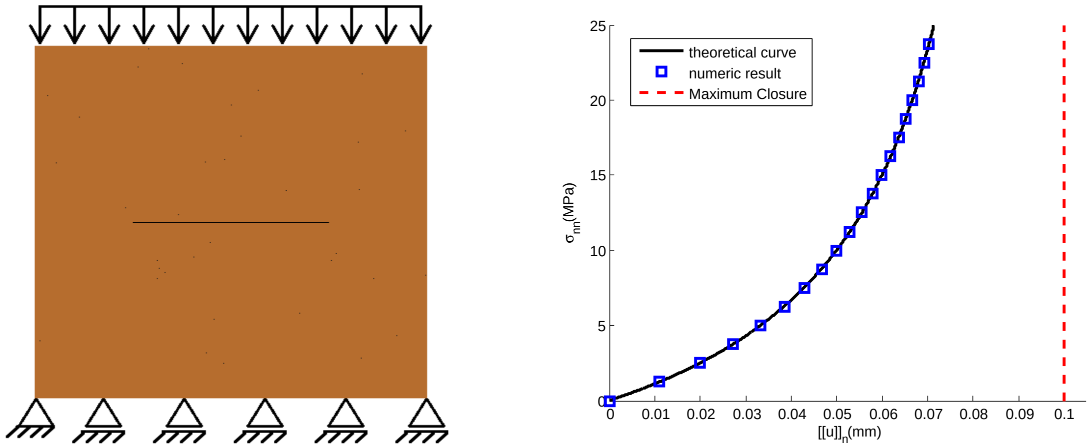

(a) (b)

Figure 5: Rock block containing a single fractured rock under compressive loading. (a) Boundary conditions. (b) Theoretical and numerical curves

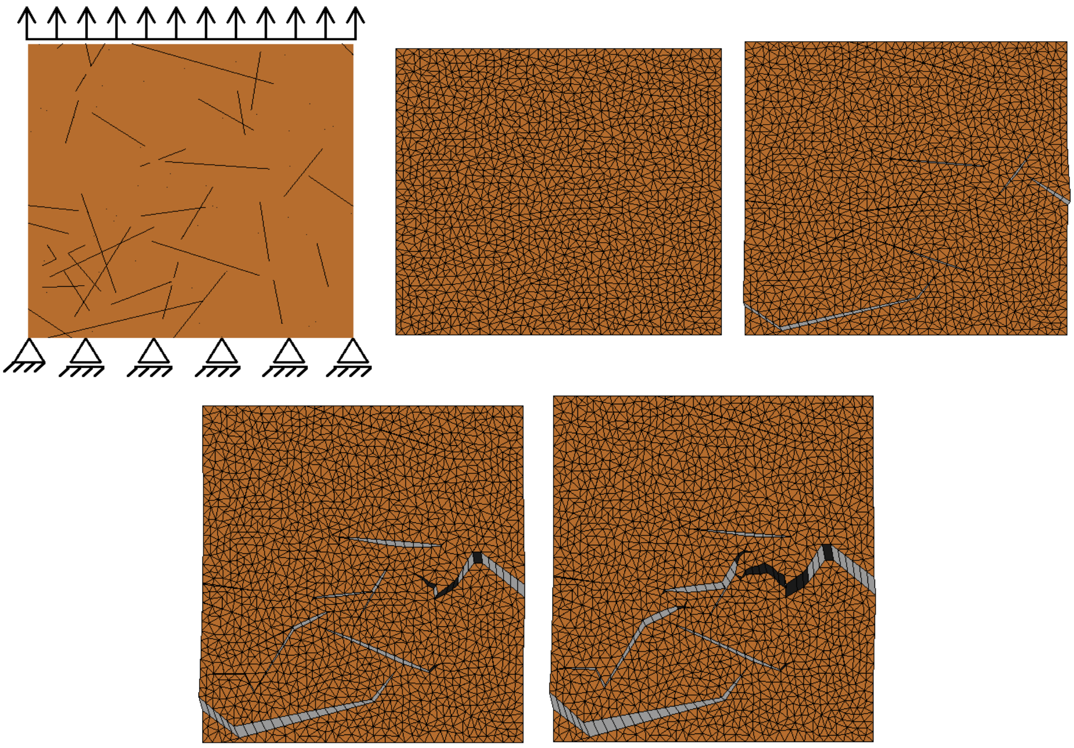

Figure 6: Rock block containing multiples fractures under tensile loading

5 CONCLUSIONS

This work presented a novel approach to simulate, on the context of Finite Elements Method, the nonlinear behavior of discontinuous rock masses. The proposed technique allies the mesh fragmentatin technique, using interface finite elements with high aspect ratio, with a proposed continuum constitutive model able to represent the behavior of the fractures.

The proposed technique showed to be able to describe both the fractures propagation and closure according to the Barton-Bandis model. Note that the effects associated with shear, as dilation, which are nown to be relevant, are not been taken into account. Therefore, more research is needed to integrate this effects on the proposed model.

Acknowledgements

The authors wish to thank the financial support provided by CAPES (Coordenação de Aperfeiçoamento de Pessoal de Nível Superior) and CNPq (Conselho Nacional de Desenvolvimento Científico e Tecnológico).

REFERENCES

Bandis, S. C., Lumsden, A. C., and Barton, N. R. (1983). Fundamentals of rock joint deformation. *Int. J. Rock Mech. Min. Sci. & Geomech*, 20(6):249–268.

Caballero, A., Lpez, C., and Carol, I. (2006). 3d meso-structural analysis of concrete specimens under uniaxial tension. *Computer Methods in Applied Mechanics and Engineering*, 195(52):7182–7195.

Camacho, G. and Ortiz, M. (1996). Computational modelling of impact damage in brittle materials. *International Journal of solids and structures*, 33(20):2899–2938.

Jager, P., Steinmann, P., and Kuhl, E. (2008). Modeling threedimensional crack propagationa comparison of crack path tracking strategies. *International Journal for Numerical Methods in Engineering*, 76(9):1328–1352.

Manzoli, O., Claro, G., Rodrigues, E., and Lopes Jr, J. (2013). A local-global scheme for tracking crack path in threedimensional solids. *COMPUTERS AND CONCRETE*, 12(3):261–283.

Manzoli, O. L., Gamino, A. L., Rodrigues, E., and Claro, G. K. S. (2012). Modeling of interfaces in two-dimensional problems using solid finite elements with high aspect ratio. *Computers & Structures*, 94:70–82.

Manzoli, O. L., Maedo, M. A., Rodrigues, E., and Bittencourt, T. N. (2014). Modeling of multiple cracks in reinforced concrete members using solid finite elements with high aspect ratio. *Computational Modelling of Concrete Structures*, page 383.

Oliver, J., Huespe, A. E., Samaniego, E., and Chaves, E. W. V. (2004). Continuum approach to the numerical simulation of material failure in concrete. *International Journal for Numerical and Analytical Methods in Geomechanics*, 28:609–632.

Pandolfi, A. and Ortiz, M. (2002). An efficient adaptive procedure for three-dimensional fragmentation simulations. *Engineering with computers*, 18(2):148–159.